Parametric Foam-Like Capacitive Sensors for 3D Printing of Deformable Parts with Sensing Capabilities

Jose Eduardo Aguilar-Segovia, Fabien Grzeskowiak, Sylvain Lefebvre, Marie Babel, Sylvain Guégan

Parametric Foam-Like Capacitive Sensors for 3D Printing of Deformable Parts with Sensing Capabilities

José Eduardo Aguilar-Segovia, Fabien Grzeskowiak, Sylvain Lefebvre, Marie Babel, Sylvain Guégan

***Abstract*— Additive manufacturing paves the way for augmenting parts with sensors fabricated in-situ, i.e. directly within the part, using functional materials deposited at the same time as the structural materials. However, achieving this goal at low cost remains challenging. This paper investigates the design of parametric capacitive sensors that can be embedded in complex designs. The sensors can be manufactured on multi-material extrusion 3D printers using commercially available non-conductive and conductive thermoplastic polyurethane. The proposed sensor consists of a parameterized foam-like structure sandwiched between two conductive plates. This allows the designer to tune both the mechanical and capacitive responses of the sensor. The effect of changing the parameters of the foam-like structure on the sensor behavior is investigated. The parametric sensors are embedded in complex parts, creating a pressure-sensitive push-button, a gamepad and an analog joystick. Conductive traces and shields are directly integrated within the components, alongside all the structural elements that form the designs. The devices are fully functional immediately after fabrication, requiring no additional processing or assembly.**

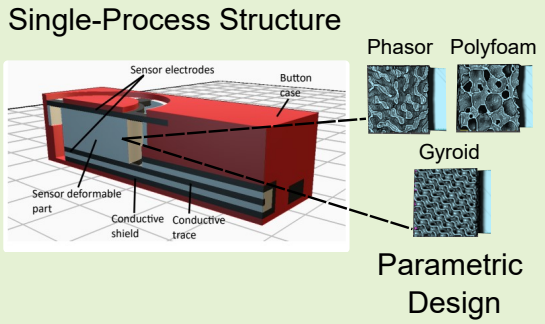

***Index Terms*— material extrusion technology, pressure sensor, capacitive sensor, single-process manufacturing.**

I. Introduction

ADDITIVE manufacturing (AM) opens exciting possibilities for fabricating complex structures within structural parts, changing their physical properties. For instance, researchers have explored ways of balancing three-dimensional (3D) structures to make them stand in a stable, up-right position [1], making internal 3D structures flexible [2], [3], shape-changing [4] or even light conductive [5].

However, these structures are limited to mechanical functions without sensing capabilities. Therefore, they can be considered passive structures [6], [7]. Embedding sensors into a 3D structure enables motion detection of parts that transmit movements from the external environment to the internal parts, e.g., the joystick handle. In addition, it allows for the identification of external interactions, such as touch or applied pressure. One approach to create interactive 3D-printed structures is to post-assemble sensors or conductive materials. For instance, Bächer et al. [8] use piezoresistive wires embedded within 3D structures to detect deformations. However, embedding sensors or conductive materials into a 3D-printed structure remains a tedious and delicate process. Material extrusion-based AM has facilitated the fabrication of sensing elements with complex structures [9], while also demonstrating its potential to produce devices with sensing capabilities in a single manufacturing process. For instance, Wang et al. [10] created an all-printed magnetic soft robot with integrated temperature, tactile and capacitive electrochemical sensing functions using multi-material direct ink writing. Košir et al. [11] introduced a piezoelectric sensor for force sensing applications. The sensor is 3D-printed using multi-material extrusion technology and is protected against electromagnetic interference. Wolterink et al. [12] create a 3D-printed soft sensor for measuring fingertip interaction forces using multi-material extrusion technology. Sotano et al. [13] have developed a 3D-printed soft finger equipped with a shape memory alloy actuator, a piezoresistive strain gauge and a capacitive sensor. The finger is manufactured using multi-material extrusion technology and a custom Cartesian pick-and-place robot to embed a shape memory alloy spring automatically.

Hence, material extrusion technology is a perfect candidate for the manufacture of sensing elements as it allows functional

This paragraph of the first footnote will contain the date on which you submitted your paper for review. This work has received funding from the Inria Defi project "DORNELL".

José Eduardo Aguilar-Segovia, Fabien Grzeskowiak and Marie Babel are with the National Institute of Applied Sciences Rennes (INSA), and also with the National Institute for Research in Digital Science and Technology (Inria) Rennes, Rennes, F-35000, France (e-mail: jose-eduardo.aguilar-segovia@inria.fr; fabien.grzeskowiak@inria.fr; marie.babel@irisa.fr).

Sylvain Guégan is with the National Institute of Applied Sciences Rennes (INSA) and also with the Civil and Mechanical Engineering Laboratory (LGCGM), Rennes, F-35000, France (e-mail: sylvain.guegan@insa-rennes.fr).

Sylvain Lefebvre is with Lorraine University and also with the National Institute for Research in Digital Science and Technology (Inria) Nancy, Nancy, F-54600, France (e-mail: sylvain.lefebvre@inria.fr;)

materials, such as flexible and conductive polymers, to be seamlessly integrated during the printing process [14]. Several approaches have been explored to create sensing elements using material extrusion technology, such as sensors based on capacitive [15]–[17], resistive [18]–[22] or piezoelectric [23]–[26] sensing. Compared to other methods, capacitive sensing has the advantages of lower power consumption and faster response time [27].

This research focuses then on the exploration of a *parametric* capacitive sensor design. The proposed sensors couple conductive electrodes and a deformable foam-like dielectric structure. The sensors are fabricated using multi-material extrusion technology and flexible conductive and non-conductive filaments. Integrating the sensors into a device enables the detection of applied pressure on the device through changes in the capacitance of the sensors. The sensors are fabricated directly within the device in a single process. As the sensors are parametric, they can be easily adapted to various application scenarios. This paper extensively studies the relationship between the sensor parameters and their capacitance and mechanical responses.

Recent works explore implementing capacitive sensing in or along *rigid* parts [6], [13], [28], as well as capturing small deformations in thin structures [29]–[31]. Schmitz et al. [32] demonstrate how to add capacitive sensing to 3D-printed passive structures by using 3D-printed internal conductive structures. However, their structures are limited to touch screens for finger detection.

Closer to the objective of this research, Gong et al. [33] integrated capacitive sensing capabilities in *mechanical metamaterial* designs. They also proposed a 3D editor in which a designer can describe the designs as an assembly of cells, which are thin-walled structures enclosing comparatively large voids. This enables a wide range of interactions between the cells and the user of the metamaterial structures, leading to the definition of intuitive physical human-machine interfaces. However, seamlessly integrating these designs into 3D shapes is challenging due to the grid-like requirement of their spatial arrangement. Furthermore, this approach does not offer the design flexibility to change the softness and capacitance range of the cell structures, as this would require changing their size.

In contrast, our work proposes a parametric sensor design, wherein the parameters of the sensor's deformable structure, such as the infill pattern, are changed in order to tune the sensor's mechanical and electrical response without modifying its size. Yu et al. [34] created pressure sensors by embedding a disk magnet into a 3D-printed deformable structure, studying the impact of the infill on sensor behavior. Nevertheless, the fabrication of these sensors requires a pause in the printing process to insert the disk magnet into the deformable structure.

It has also been demonstrated that structures similar to foams can be used to create *resistive* sensors, printing deformable periodic truss [35] or gyroid structures [36] with flexible conductive filaments. However, flexible conductive thermoplastic polyurethane (TPU) filament is stiffer than its non-conductive counterpart and more complex to print reliably, in particular on truss structures that create many isolated islands within every slice. Some other works rely on post-processing to make the structure conductive [36], [37]. This post-processes impacts the printing process and prevents the sensor from being combined in multi-material layouts. In contrast, in our research, the deformable foam is printed in non-conductive flexible filament, using *closed* cell foams. This enables the use of more flexible materials while printing reliability and imposes less strict requirements on printing accuracy. Indeed, 3D printing of deformable structures is challenging on filament processes, and print defects impact electrical measurements. Truss networks in particular – as used in [35], [37] – are known to be problematic with material extrusion technology: the trusses are sliced as disconnected and small extrusion islands in each layer. These structures are particularly difficult to fabricate as the extrusion process stops and resumes many times per layer – once per island – leading to extrusion defects and filament grinding, see e.g. [2] for details. The vertical layering along beams also damages conductivity as inter-layer bonding is weaker. In contrast, our method relies on closed-cell foam structures that are printed as continuous trajectories with few travel moves. This foam structure is then used to create a flexible dielectric foam between two conductive plates. In addition, only the conductive plates are printed in *conductive* filament: their simple plate geometry is indeed ideal for deposition. This paper explores then the use of internally deformable foam-like 3D-printed structures to fabricate sensing elements able to sense pressure over a wide range (90 Pa - 170 kPa) to create deformable devices in a single manufacturing process. Our approach uses an affordable multi-material extrusion 3D printer. The complex deformation behaviors triggered by functional infill patterns – foam-like structures with anisotropic responses – are then exploited to enable mechanical interactions. This research aims to provide a proof of principle that the elastic properties and pressure sensitivity of 3D printed capacitive foam-like sensors can be controlled by modifying the parameters of their dielectric structure, e.g. the infill structure. This adaptability allows the proposed capacitive sensors to be used in various applications requiring rigid or flexible sensors. Furthermore, the seamless integration of these sensors into complex structures such as a push button, a game pad and a joystick is also demonstrated. All devices are fabricated with single-process, multi-material 3D printing.

II. Materials and Methods

This section describes the design and fabrication of the foam-like capacitive sensor and explains its sensing principle. It also presents the experimental analysis carried out to study how changes in the parameters of the sensor dielectric foam affect its behavior and to identify the sensor characteristics.

A. Sensor design and fabrication

The proposed capacitive sensors are designed in a parametric modeling software called IceSL [38]. All the sensors share the same dimensions: the size of the electrodes is 30 mm $\times$ 20 mm $\times$ 1 mm (last value corresponds to the thickness) and the size of the dielectric foam is 20 mm $\times$ 20 mm $\times$ 10 mm. The electrodes are printed with a density percentage

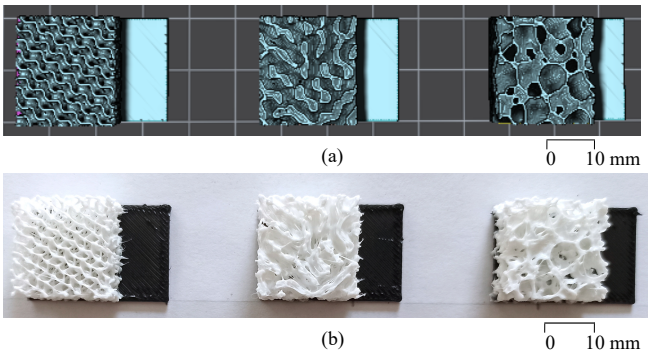

Fig. 1. The three different infill patterns available in the IceSL software **(a)**, along with their corresponding manufactured versions **(b)**. From left to right: Gyroid, Phasor and Polyfoam infill.

of 100%, while the dielectric foam structure is created using three different microstructures, as shown in Fig. 1.

- Phasor Infill: The technique implemented in the IceSL software to create the phasor infill was introduced by Tricard et al. [3]. The 3D microstructure geometry of the infill is defined from a stochastic pattern generator that produces sharp and contrasting oscillating patterns. This technique allows the designer to manipulate the orientation and the anisotropy of the resulting 3D foam structure and can generate very flexible patterns. This infill pattern is designed to print reliably on 3D printers.
- Polyfoam Infill: The polyfoam infill is created using the technique presented by Martínez et al. [39]. This technique uses polyhedral Voronoi diagrams to generate a fabricable, stochastic microstructure, forming a closed-porous foam. The size and shape of the porous can be spatially varied in the plane parallel to the printer bed.
- Gyroid Infill: The 3D microstructure geometry of the gyroid infill is constructed by continuous curvilinear movements during material deposition. This infill is typical in AM and known for its near isotropic behavior [5] [40].

The sensors are fabricated using a multi-material extrusion 3D printer (ToolChanger, E3D Inc.) with four independent extruders, each with a nozzle diameter equal to 0.4 mm (Revo Hemera., E3D Inc.). The dielectric foam is printed using TPU 60A (Filaflex 60A 'PRO', RECREUS), a flexible TPU filament. The electrodes are made of a flexible conductive filament (Conductive Filaflex TPU, RECREUS).

B. Background on sensing principle

When a pressure P perpendicular to the axis of the electrodes is applied to the deformable sensor, it causes a change in the sensor geometry, leading to a corresponding change in the sensor capacitance value.

Let z_0 be the thickness of the sensor, d the deformation displacement of the electrodes, ε_0 the electrical permittivity of free space, ε_r the dielectric permittivity of the non-conductive material and A the relative area. Then the capacitance C is linked to the displacement of the electrodes [41] by

$$C = \frac{\varepsilon_0 \varepsilon_r A}{z_0 - d}. \tag{1}$$

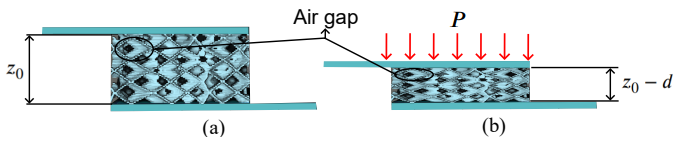

Fig. 2. Schematic representation of the sensor sensing principle. Capacitive sensor without pressure **(a)**, and capacitive sensor under an applied pressure P **(b)**. When pressure is applied to the sensor, the dimensions of the air gaps and the distances between electrodes are reduced, leading to an increase in capacitance.

Adding air gaps in the dielectric slab – the non-conductive part sandwiched between the electrodes – significantly reduces its permittivity. In this work, the dielectric slab is made of foam, so that during loading, the volume ratio of the air gaps in the foam decreases while that of the non-conductive material increases (Fig. 2). This leads to a change in the dielectric foam permittivity. However, to the best of our knowledge, there is no analytical model that expresses the dielectric permittivity of a thermoplastic foam as a function of the force vector during compression. In addition, factors such as temperature or the operating frequency can also affect the dielectric properties of the material [42]. Even though some studies have tried to precisely describe the characteristics of elastomers, they are restricted to the case of homogeneous materials [43] [44].

Nevertheless, it can be considered that the dielectric foam permittivity can be approximated by combining the dielectric permittivity of the non-conductive material and that of air in the gaps between the electrodes. Let θ be the volume ratio of air, ε_{air} the dielectric permittivity of air and ε_s the dielectric permittivity of the dielectric foam [45] such that

$$\varepsilon_s = \varepsilon_r\big(1-\theta\big) + \varepsilon_{air}\big(\theta\big). \tag{2}$$

Therefore, if ε_r in equation (1) is replaced by ε_s expressed by equation (2), and considering that the contact area of the capacitor remains constant and equal to the sensor's top surface area during loading, the capacitance can be written as

$$C = \frac{\varepsilon_0 \varepsilon_r \big(1-\theta\big) A}{z_0 - d} + \frac{\varepsilon_0 \varepsilon_{air} \theta A}{z_0 - d}. \tag{3}$$

Thanks to equation (3), it can be deduced that the capacitance depends on the relative permittivity of the non-conductive material, the volume ratio of air gaps, the relative area, and the deformation of the sensor.

Considering that C_0 is the capacitance of the sensor without pressure and ΔC is the capacitance change during compression, the pressure sensitivity, denoted by S, is defined as

$$S = \frac{\delta\left(\frac{\Delta C}{C_0}\right)}{\delta P}, \tag{4}$$

with $\frac{\Delta C}{C_0}$ being the relative capacitance change. From equations (3) and (4), it can be stated that the dielectric foam's mechanical properties impact the sensor's pressure sensitivity. Hence, the foam's parameters (infill, density and anisotropy) and the mechanical properties of the material used to fabricate it affect the sensor's mechanical and capacitance response. In this study, the foam structure is printed using TPU, which

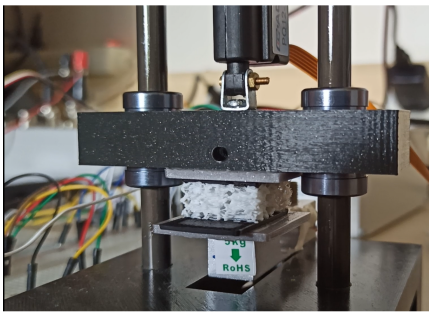

Fig. 3. Compression test bench machine. A linear actuator compresses the capacitive sensor while measuring its deformation in the z-axis. An external force sensor measures the compression force, and a capacitance to digital circuit measures the capacitance of the sensor during loading. All the data is sent to a control board.

has a molecular structure comprising hard and soft segments, resulting in a two-phase morphology, see e.g. [46] for details. The molecular structure of the TPU results in the material exhibiting strong hysteresis, time dependence, and cyclic softening in its stress-strain ($\sigma - \gamma$) behavior [46]. Specifically, at room temperature, the hard segments lead to strong hysteresis, permanent deformation, and an increase in tensile strength and modulus, whereas the soft segments cause restitutive behavior under deformations, see e.g. [46], [47] for details. In our context, the compressive stress σ is equal to the pressure P, and the strain γ is equal to the ratio of the deformation displacement of the electrodes and the thickness of the sensor ($\frac{d}{z_0}$), during sensor deformation.

C. Experimental setup

Several experiments were conducted to investigate the overall characteristics of the proposed capacitive sensors. Pressure tests were conducted to observe the relationships between strain, stress, and relative capacitance change. In addition, humidity and temperature tests were also conducted to investigate their influence on the sensor performance.

Across compression experiments, the foam structure parameters were modified to obtain a wide variety of geometries. In particular, the foam density is adjusted – or equivalently, the length of filament used for 3D printing the foam is adjusted. For this purpose, a compression test bench has been designed. The compression tests were performed at room temperature and in a well-ventilated room.

Fig. 3 shows the compression bench machine used for the compression tests. A linear actuator (PQ12-P, Actuonix) is used to apply loading-unloading cycles to the sensors. This actuator includes a potentiometer position feedback that indicates the actuator position. A capacitance-to-digital circuit (FCD1004, ProtoCentral) is used to measure capacitance. This circuit can be configured to operate at an internal sampling frequency of up to 400 Hz. However, as lower sampling frequencies provide higher sensitivity and resolution in the capacitance measurement [29], the lowest internal sampling frequency of the circuit was selected, which is 100 Hz. Force measurement is performed using a 5 kg load cell (CZL635-5) and a load cell controller (HX711). The force measurement was calibrated using calibration weights. The force transducer was used with an internal sampling frequency of 10 Hz. Thus, the sampling frequency of the compression system was 10 Hz. A microcontroller (ESP32 Basic Core, M5Stack) is also used to measure force and capacitance values. These values are then sent to a controller board (DS1104 R&D Controller Board, dSPACE). The controller board also reads the analog position feedback from the linear actuator via its integrated 16-bit analog-to-digital converter (ADC) and sends the desired input position signal to the linear actuator control board via its internal 16-bit digital-to-analog converter (DAC).

D. Procedure and data collection

Before conducting a characterization experiment, the sensors used in the test were subjected to a preconditioning test of a thousand loading-unloading cycles at an applied pressure of approximately 82 kPa (approximately 75% of the maximum pressure supported by the load cell). Indeed, it was observed that during the first cycles, the sensors exhibited a slightly stiffer behavior compared to their performance after the preconditioning test. After approximately five hundred cycles, the sensors exhibit a stable response. This phenomenon can be attributed to the softening behavior of TPU [46].

For the characterization tests, the measurements of each sensor were averaged over ten loading-unloading cycles, with a pressure range of 0-110 kPa. This pressure range was chosen to respect the measurement range of the load cell. The minimum pressure that the sensors could detect is 90 Pa. We decided to compress the sensors at a strain of about 0.6 since up to this strain, the most flexible sensor – the sensor based on phasor infill with 0% anisotropy – (see Section III-C) can be reasonably deformed with $\theta \approx 0$. Nevertheless, we experienced that the most rigid sensor – the sensor based on polyfoam with a volume of non-conductive material of 1.47 cm^3 – (see Section III-B), could be reasonably deformed up to 170 kPa. This range could be extended by changing the material used to fabricate the dielectric foam to a more rigid material or using higher-density capacitive sensors than those tested in our study. Force, capacitance, and sensor deformation were measured for all the tests. The sampling rate was equal to 10 Hz, capturing 50 data points for each loading-unloading cycle (5 seconds per cycle).

The effect of changing the dielectric foam infill on sensor behavior is first explored by testing three sensors with polyfoam, phasor, and gyroid infill with the same density. Then, 12 sensors are tested to study the effect of density. For each infill, four sensors with different densities are considered.

As anisotropy can be controlled in sensors based on phasor infill, the influence of this parameter on the sensor's mechanical and capacitive response is investigated; five sensors are evaluated with anisotropy percentages from 0% up to 100%.

Next, the strain rate influence on the sensor's mechanical and electrical behavior is studied. Since the 3D-printed microstructures may degrade over time, the durability and stability of the sensor is evaluated by conducting a 7200 cycles test, corresponding to ten hours.

Next, consistency across prints is investigated. To this aim, five sensors were fabricated using the same G-code, and their mechanical and electrical responses were compared.

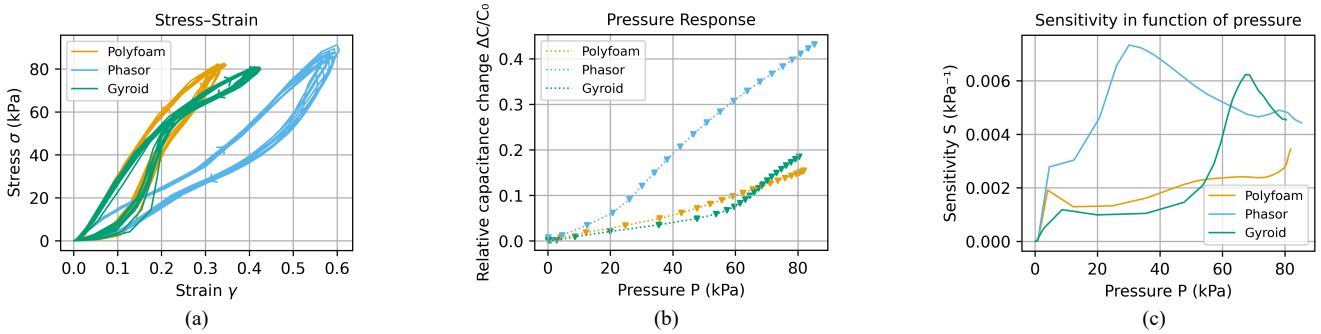

Fig. 4. Evaluation of the influence of the sensor's dielectric foam geometry on its behavior. (**a**) Stress-strain curves for three sensors with different dielectric foam geometrical structures but same dimensions and volume of non-conductive material V_m = 1.02 cm^3. (**b**) Corresponding pressure-response curves. (**c**) Corresponding sensitivity curves.

Finally, the effect of temperature and humidity on the sensor behavior is examined by testing three sensors, each with phasor infill but with different densities.

For the strain rate influence test, durability test, consistency test, humidity test and temperature test, sensors based on isotropic phasor infill were used to perform the tests. This infill was used because of its complex structure with variable oscillating patterns.

III. Results

Several compression-relaxation tests were conducted to evaluate the overall characteristics of the capacitive sensor. The sensitivity was assessed with regard to infill, the volume V_m and the anisotropy percentage. The results of these tests are presented and analyzed in the followings.

A. Infill influence

To evaluate the sensitivity with respect to infill structure, a test was conducted using three sensors, each sensor having a non-conductive volume material equal to 1.02 cm^3. In the stress-strain curve shown in Fig. 4 (**a**), it can be observed that the sensor with phasor infill exhibits higher flexibility compared to the other two sensors, while the sensor employing polyfoam infill demonstrates the least flexibility. The pressure-response curves are depicted in Fig. 4 (**b**). It can be observed that the capacitive sensor with a dielectric foam based on phasor infill exhibits a higher relative capacitance change than the other two sensors. Fig. 4 (**c**) indicates that the sensor based on phasor infill exhibited the highest sensitivity value compared to the other two sensors, and higher sensitivity values in the pressure range of 0–62 kPa.

B. Dielectric foam density influence

This section aims to determine the impact of dielectric foam density on the sensitivity of sensors with different types of infill through various tests.

a) Sensors with dielectric foam based on phasor infill: In this part, the impact of varying the sensor density based on phasor infill on its behavior is investigated. All the sensors used in the loading-unloading tests had an isotropic dielectric foam.

The stress-strain curves are depicted in Fig. 5 (**a**). As expected, denser sensors are stiffer. The pressure response curves and sensitivity curves are depicted in Fig. 5 (**b**) and (**c**), respectively. In Fig. 5 (**b**), it can be observed that as the density of the sensor dielectric foam increases, the range of capacitance produced by the sensor decreases. In addition, Fig. 5 (**c**) indicates that for higher sensor density, the maximum point value on the bell-shaped sensitivity curve decreases while the pressure at which this point is reached increases. Overall, higher-density sensors are less sensitive and less flexible. This provides a wide range of possibilities for controlling the sensitivity of the sensor and the force exerted by users to deform it.

b) Sensors with dielectric foam based on polyfoam infill: The results are shown in Figs. 5 (**d**), (**e**) and (**f**). The related stress-strain curve is shown in Fig. 5 (**d**). The presented stress-strain curve shows that an increase in material volume reduces sensor flexibility. This behavior is similar to that observed in sensors with a dielectric foam based on phasor infill.

Fig. 5 (**f**), shows that the sensitivity of the sensors based on polyfoam infill decreases as the volume V_m increases. Furthermore, increasing sensor stiffness reduces sensitivity variations, resulting in a near-constant sensitivity value.

c) Sensors with dielectric foam based on gyroid infill: The results are depicted in Figs. 5 (**g**), (**h**) and (**i**). Fig. 5 (**g**) indicates that the sensors based on gyroid infill exhibit the same mechanical behavior as the other groups of sensors. As the dielectric foam density of the sensor increases, its flexibility decreases. In Fig. 5 (**h**), it can be seen that the shape of the pressure response curves is similar to that of the stress-strain curves. In addition, in Fig. 5 (**i**), it can be observed that the shape of the sensitivity curves is similar to that of sensors with dielectric foams based on phasor infill. The maximum sensitivity value increases when the dielectric volume material decreases. Nevertheless, compared to the sensors using phasor infill, the maximum sensitivity value is reached at higher pressures. This further demonstrates the influence of the dielectric foam's geometrical structure on sensor sensitivity.

C. Dielectric foam anisotropy percentage influence

This section examines the impact of varying dielectric foam anisotropy on sensor behavior. To prevent the volume of non-conductive material from influencing the sensor response, all

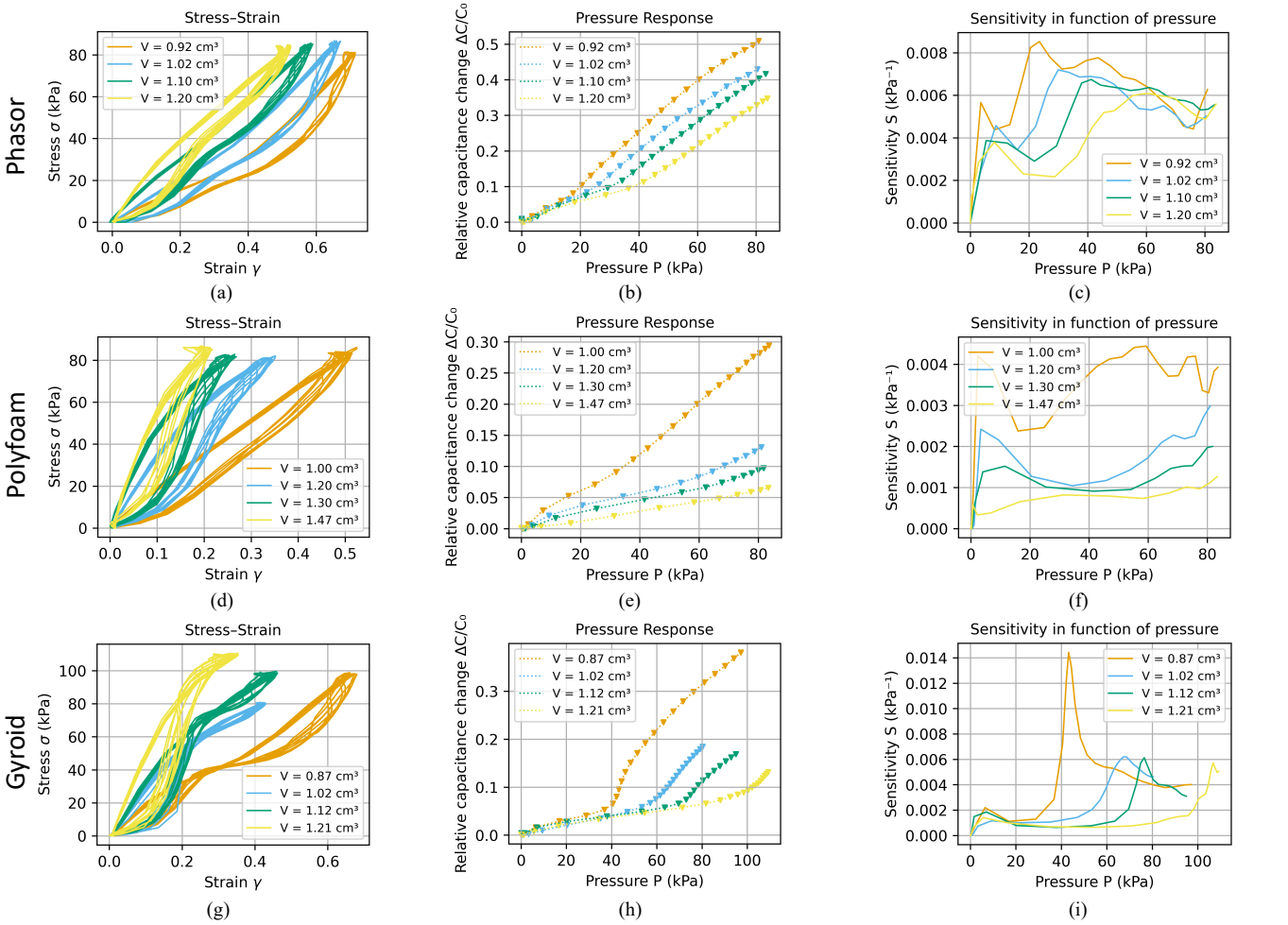

Fig. 5. Dielectric foam density impact on sensor behavior. (**a**)(**d**)(**g**) Stress-strain curves for the three groups of sensors at different densities: phasor, polyfoam, and gyroid infill. (**b**)(**e**)(**h**) Corresponding pressure-response curves. (**c**)(**f**)(**i**) Corresponding sensitivity curves.

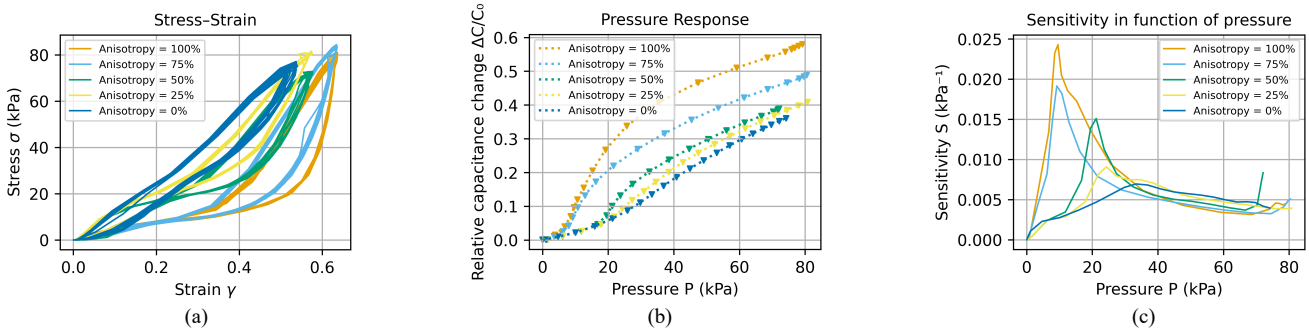

Fig. 6. Dielectric foam anisotropy percentage influence on sensor behavior. (**a**) Stress-strain curves for the sensors based on phasor infill with different anisotropy percentages and the one with isotropic properties (0% anisotropy). (**b**) Corresponding pressure-response curves. (**c**) Corresponding sensitivity curves.

the sensors are printed at the same volume of non-conductive material, i.e. V_m = 1.02 cm^3. Five sensors with anisotropy percentages equal to 0%, 25%, 50%, 75% and 100% are tested.

Thanks to the stress-strain curve depicted in Figs. 6 (**a**), it can be seen that sensors with anisotropy percentages equal to 75% and 100% have similar stress-strain behavior. Indeed, at high anisotropy levels, there are only minor differences in the geometric features of the sensor. Nevertheless, it can also be seen that increasing the anisotropy percentage will increase the sensor flexibility. The pressure response and sensitivity curves are shown in Figs. 6 (**b**) and (**c**). It can be observed that while the anisotropy percentage impacts capacitance and sensitivity, this impact is much smaller than that of a change in density (Section III-B). In particular, it can be seen that after 50 kPa, the anisotropy percentage no longer influences the sensor sensitivity, which remains approximately the same. This indicates that anisotropy can be controlled without significantly changing the sensor response.

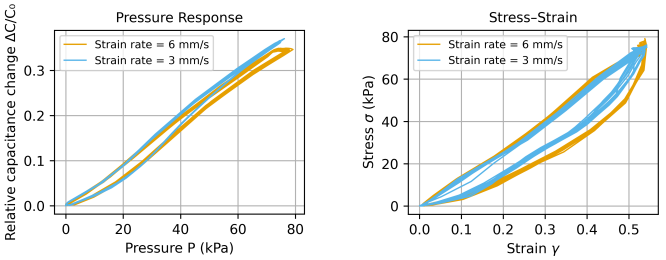

Fig. 7. Strain rate influence on sensor behavior.(**a**) Relative capacitance change as a function of pressure. (**b**) Corresponding stress—strain curves.

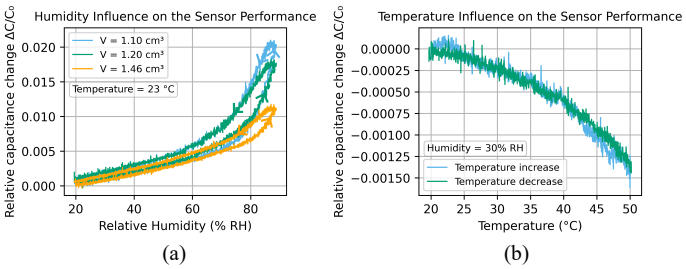

Fig. 8. Temperature and humidity influence on sensor behavior. Relative capacitance changes as a function of humidity (**a**), and Relative capacitance changes as a function of temperature (**b**).

D. Strain rate effect on sensor behavior

To evaluate the effect of the strain rate applied to the sensor, two loading-unloading tests were conducted: one at a strain rate of 6 mm/s and another at 3 mm/s. The sensor to be tested had a dielectric foam based on phasor infill, isotropic, and with a volume of non-conductive material equal to 1.20 cm^3.

Fig. 7 shows the pressure response curves and the stress-strain curves at different strain rates. It can be seen that the unloading part of the curves from different strain rates are very similar. In the case of the loading part of the curves, an increase in strain rate will result in an increase in stress, as shown in [46]. Regarding the pressure response curve, it can be observed that an increase in the strain rate leads to a decrease in the relative capacitance change.

E. Durability and stability

The sensor performance was evaluated over 7200 loading-unloading cycles, corresponding to ten hours, while applying a pressure of approximately 82 kPa. The sensor used for the test had a dielectric foam based on phasor infill, isotropic, and with a volume of non-conductive material equal to 1.20 cm^3.

After the durability test, no evidence of material fatigue was identified. Indeed, the maximum values of deformation remained approximately equal to 5 mm, and the maximum values of relative capacitance change remained approximately equal to 0.30. In fact, our approach avoids deforming fragile conductive structures: the dielectric foam that absorbs the deformation is fabricated with a non-conductive flexible filament. This method avoids durability issues classically associated with deformable sensors manufactured with flexible conductive filaments, such as resistive sensors, where resistance decreases by deformation rates over time [35].

F. Consistency test

An experiment was conducted to evaluate consistency across prints. Five sensors were printed using the same G-code, and then tested to compare their mechanical and electrical responses. The sensors had an isotropic dielectric foam based on phasor infill with a volume of non-conductive material equal to 1.20 cm^3. It was identified that neither the stress-strain behavior nor the pressure response of the sensors exhibited any significant alterations across the prints.

G. Temperature and humidity influence on sensor behavior

This section examines the impact of temperature and humidity on the sensor's response. The temperature and humidity tests were conducted using an environmental test chamber (CTC256, Memmert) and the capacitance measurement system described in Section II-C. Three capacitive sensors, each with an isotropic phasor infill and a volume of non-conductive material of 1.10 cm^3, 1.20 cm^3 and 1.46 cm^3, respectively were used for the tests. For the humidity test, the sensors were subjected to a linear increase and decrease in humidity ranging from 20% RH to 90% RH over sixteen hours at a constant temperature of 23°C. In the temperature test, the sensors were exposed to a linear increase and decrease in temperature, ranging from 20°C to 50°C over eight hours at a constant relative humidity of 30% RH.

Fig. 8 (**a**) shows the results of the humidity test. It can be observed that as the relative humidity increases, the relative capacitance change increases. Conversely, a decrease in humidity results in a decrease in the relative capacitance change. In addition, the relative capacitance change-relative humidity curve exhibits a hysteresis effect. This could be attributed to the hygroscopic properties of TPU [48], the moisture absorption in the dielectric foam's air gaps, and an increase in the dielectric permittivity of the TPU as humidity increases, which has also been observed in other elastomers [49]. In addition, sensor density was found to affect the relative capacitance change-humidity behavior: as sensor density increases, the sensor is less sensitive to humidity changes and exhibits fewer relative capacitance changes than lower density sensors.

Regarding the effect of temperature on sensor performance, it was identified that density does not affect the relative capacitance change-temperature relationship. Fig. 8 (**b**) shows the results for the sensor with a volume of non-conductive material equal to 1.10 cm^3. It can be seen that the relative capacitance change decreases as the temperature increases. Conversely, a decrease in temperature results in an increase in the relative capacitance change. At the maximum temperature of 50°C, the relative capacitance change is equal to -0.00145. This phenomenon can be attributed to a decrease in the dielectric permittivity of the TPU as temperature increases; it has also been observed in other elastomers [50].

H. Sensor design guidelines

The analyses of the experimental results lead us to propose sensor design guidelines, with the aim of successfully embedding capacitive sensors into complex devices.

At a given sensor thickness, the capacitive response is mainly influenced by the foam density, while the foam anisotropy has a much lower impact. Hence, a low foam density will provide a wide range of capacitance values with high sensitivity, and is recommended for precise interactions. Conversely, a high-density sensor is recommended for larger deformations inducing higher stresses, e.g. when an external mechanical device applies a significant effort on the sensor. Given its minimal impact on the capacitive response, the anisotropy can be freely controlled to influence the device's flexibility at near-constant sensitivity.

When selecting a capacitive sensor, the choice of parameters will depend on the specific application. Based on the stress–strain curves, it can be concluded that sensors with dielectric foams based on anisotropic phasor infill exhibit higher flexibility than the other sensors. Furthermore, sensors with dielectric foams based on phasor infill demonstrated higher sensitivity than those with dielectric foam based on polyfoam or gyroid infill.

If an application needs the sensor to be more flexible or sensitive, designers may want to decrease sensor density. However, as indicated by equation (3), a substantial reduction in the density of the material will result in an increase in the volume ratio of air θ. Consequently, this would induce a significant reduction in the dielectric permittivity of the non-homogeneous foam and, as a result, a substantial decrease in the capacitance of the sensor. In this case, designers may preferably consider decreasing the anisotropy percentage of the dielectric foam instead of the density.

When a designer requires a rigid sensor, it is advantageous to use a sensor with a polyfoam infill structure, as it exhibits less flexibility compared to sensors based on gyroid or phasor structures. In addition, the polyfoam sensor exhibits less variation in sensitivity compared to sensors using gyroid patterns, with less variation in the stress-strain behavior.

IV. Applications

This section highlights the fundamental principle of integrating foam-like capacitive sensors into 3D structures. In order to demonstrate the effectiveness of our approach, a force-sensitive push-button, a gamepad, and a full analog joystick are created. All embedded sensors are analog and measure continuous pressure information. In each case, the key point lies in the cost-effective and efficient fabrication of these devices within a single manufacturing process: each device is operational right out of the printer without any further assembly process. A program created in IceSL software was used to design a push button and a gamepad. The program enables users to interactively set the number of buttons (from one to five), the dimensions of the buttons, the density, and the anisotropy percentage of the sensor's dielectric foam can be selected through sliding bars. The joystick was designed using Fusion 360 software. IceSL software was also used to establish the printing characteristics, infill patterns of the parts comprising the devices, and generate the G-code.

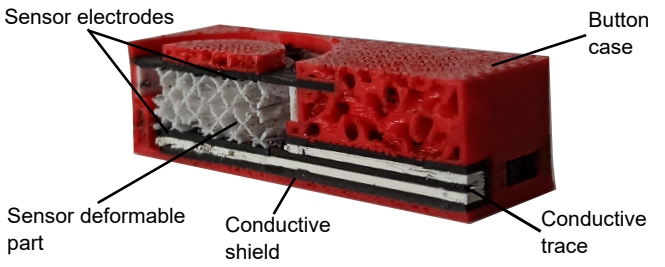

Fig. 9. Longitudinal section of the push-button design, in the manufactured version, with notations. The push-button is fabricated in a single 3D print and consists of a capacitive foam sensor, conductive traces, conductive shields, and a case.

Each device consists of three functional structures: the foam sensors, the conductive shields and traces, and other mechanical structures as shown on Fig. 9. The conductive traces are used to connect the sensors' electrodes to conductive pads located on the surface of the device. The shield structures are added to reduce environmental electromagnetic noise. The conductive shields and traces are printed using conductive filament. The conductive shields are electrically isolated from the conductive traces and the sensor electrodes thanks to an insulating structure printed with a thermoplastic elastomer (TPE) insulating filament (Ice9 E-Insulating Flex TPE, TCPoly).

The devices are fabricated using the E3D ToolChanger 3D printer. Once printed, the device sensors are connected to the capacitance measurement system using shield wires that are connected to the device's conductive traces. The shield wires are connected to the device by heating them with a soldering iron and forcefully inserting them into the conductive pads. Once connected to the capacitance measurement system, the device is ready to be used. The power consumption while measuring the capacitance change of the button (single capacitive sensor) was 1.8 Wh. This consumption could be lowered by using another microcontroller with short start-up times and lower power consumption. As with most analog devices, a calibration step is required for the devices before use.

A. Button and gamepad

The button has dimensions of 55 mm $\times$ 32 mm $\times$ 15 mm. The button case is fabricated using Red TPU 95A (Filaflex 95A, 'Medium-Flex', RECREUS). The button sensor is cylindrical with a diameter of 20 mm, and the dielectric foam has a thickness of 8 mm. The pattern for the dielectric foam is a phasor infill with an anisotropy percentage equal to 50%. To create a "spring" behavior when pressing the button, four *lamellae* made of conductive filament are added to the top electrode as depicted on Fig. 9.

The capacitance measure is sent from the microcontroller to a PC terminal by serial communication. In the PC terminal, the color of a circle changes, using the viridis color map scale to indicate the relative capacitance change value. Fig. 10 shows the 3D printed button and three operational states:

- the *off* state, where the button remains untouched, the relative capacitance change is equal to 0,

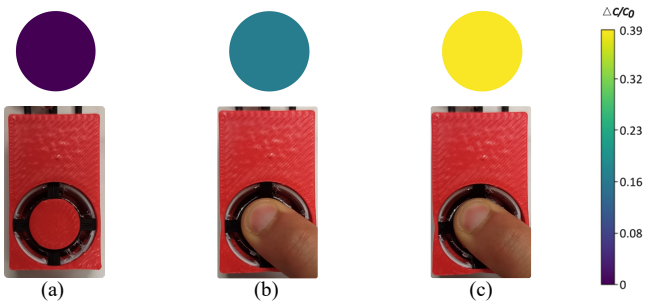

Fig. 10. The 3D printed button being pressed by a finger, showing three different states: *off* state when the relative capacitance change is equal to 0 (**a**), *partially pressed* when the relative capacitance change is equal to 0.17, (**b**) and *completely pressed* when the relative capacitance change is approximately equal to 0.39 (**c**).

- the *partially pressed* state, where the relative capacitance change is equal to 0.17,
- the *completely pressed* state where the relative capacitance change is approximately equal to 0.39.

As a second, more elaborate example, a gamepad with four buttons is fabricated. The dimensions of the gamepad are 114 mm × 114 mm × 26 mm. The gamepad case is fabricated using Yellow TPU 82A (Filaflex 82A, 'Original', RECREUS). To demonstrate how the system works, a ping-pong game was created. Two buttons are used for one player and the other two for another player (Fig. 11 (**a**)). The buttons are used to control the direction and the speed of the plates in the game (Fig. 11 (**b**)). In this case, capacitance values are used to detect the direction and the speed.

B. Analog joystick

To illustrate the potential of the foam-like capacitive sensors for the fabrication of complex electronic devices, a complete analog joystick created in a single manufacturing process is proposed. The dimensions are 106.55 mm × 106.55 mm × 102.84 mm. The joystick case, the joystick handle and the button cover are made from yellow TPU 82A (TPU Filament Filaflex 82A, 'Original', RECREUS). Fig. 12 (**a**) and Fig. 12 (**b**) illustrate respectively a longitudinal cut of the 3D model and the bottom view. This integrated design combines the case, five sensors, conductive traces, conductive shields, electrical insulators, a joystick handle, a button cover and a TPU joystick boot. The design is printed using four different materials. Fig. 12 (**c**) shows the sensors, the conductive traces, the conductive shields and the electrical insulators between them. To connect the joystick to the sensor measurement circuit, shielded wires are connected to its bottom.

Fig. 12 (**d**) shows the manufactured version of the joystick. Four sensors, one in each direction (up, down, left, right), are used to detect the direction indicated by the joystick position. The joystick can also be pressed following the negative z-axis; in this case, the four sensors are pressed at the same time. An additional sensor is used to create a button, following the principle presented in the previous section. An 8-channel I2C bus switch (PCA9548A) is used to control two capacitance measurement circuits on the same I2C bus.

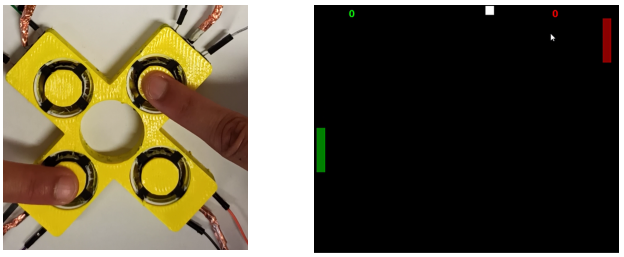

Fig. 11. Gamepad used in a PONG game. (**a**) The two left buttons control the green pad and the two right buttons control the red pad. (**b**) The gamepad is used to sense the pressure applied on the buttons in order to control the direction and speed of the pads on the game.

The microcontroller interprets the capacitance values from the sensors into signals that describe the stick's movement.

Fig. 12 (**e**) illustrates the use of the joystick to move a digital circle on the ESP32 Basic Core screen. Fig. 12 (**f**) shows that the radius of the circle increases when the joystick shaft is pressed. Note that when the joystick button is pressed, the color of the circle changes to red.

V. Limitations and Future Work

a) Mechanical characteristics of the structures: The devices presented in this paper have embedded sensors that measure deformation applied externally, e.g., by a user's hand or finger or by an external mechanism. Extensive analysis of the sensors is provided in isolation to determine design guidelines (Section III-H). However, it should be noted that the surrounding structures influence the sensor stress-strain behavior when embedded in complete designs. To limit this effect, an empty space is left around the sensors and connected with conductive *lamellae* to the traces within the design (Fig. 9, top lamellae).

b) Geometric sizing requirements: In the preceding sections, it was demonstrated that foam-like sensors can be printed simultaneously with a 3D design using a multi-material 3D printer. The minimal size of the sensors is constrained by the resolution and the nozzle diameter of the current commercial multi-material 3D printers. Using our setup, the minimal thickness of the electrodes is 0.8 mm, i.e. four 0.2 mm layers. Using four layers ensures that the top electrode of the sensor is fully formed and filled. In addition, the maximum size of sensor electrodes is limited by the low conductivity of the material. Conductor lengths of up to 23.6 cm and electrodes with an area of up to 400 mm^2 were successfully tested without observing any effect on sensing performance. However, it is recommended that designers construct conductive structures as large as necessary for their intended use. Future research will determine a range of sizes of conductive structures.

Furthermore, it was determined that the spacing between the conductive parts and the shield has to be around 1 mm for horizontal layers and 2 mm for vertical layers. This avoids unwanted electrical connections between traces/electrodes and the shield. Specialized deposition methods could improve this in the future. Finally, designers are discouraged from increasing the sensor thickness since $C \propto \frac{A}{z_0 - d}$, see Section II-B. The experiments show that pressure variations can be successfully detected within a sensor thickness of ≤ 10 mm.

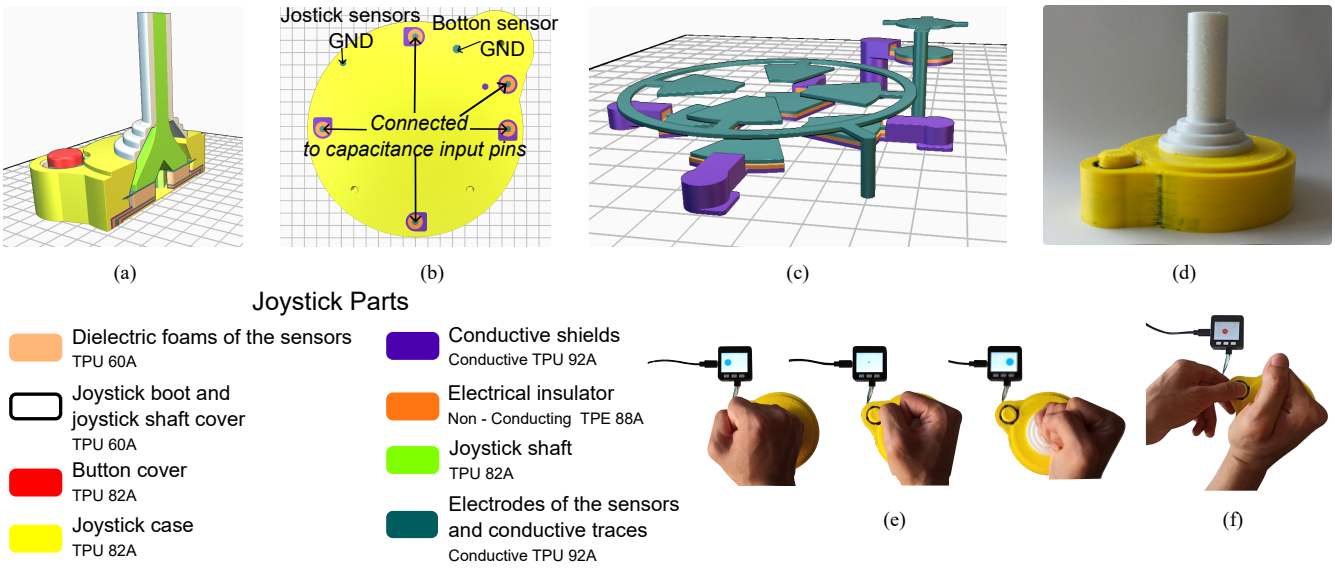

Fig. 12. Details of the 3D printed analog joystick. (**a**) 3D model of the joystick with a longitudinal cut, (**b**) joystick bottom view, (**c**) sensors with their respective conductive traces and (**d**) manufactured version of the joystick. (**e**) When the joystick shaft is manipulated, the circle on the screen is moved correspondingly, e.g., to the left or right. (**f**) The circle's radius increases when the joystick is pressed. The circle's color changes when the button of the joystick is pressed.

c) Grounding conditions: As any capacitive measurement systems, the performance of the sensors may be influenced by grounding conditions, particularly when the devices are connected to larger ground planes. This was not found to be an issue in practice. Additional conductive structures could be added to the 3D structure to further mitigate disturbances.

d) Effects of external electric fields on sensor behavior: The electrical response of the capacitive sensors can be affected by external electric fields, which can result from external electrical devices operating nearby or by human movement due to static charging [51]. In the case of our devices (Section IV), environmental electromagnetic noise did not influence their response, as the sensors' electrodes and the conductive traces embedded in the devices are shielded and covered with an insulating material. Nevertheless, as future work, further research will be conducted to test the shielding efficiency.

e) Effects of temperature and humidity on sensor behavior: As previously identified in Section III-G, variations in the sensor's temperature will slightly change its response. In contrast, variations in the sensor's humidity significantly impact the sensor response. Therefore, when implementing the sensors in an application where humidity or temperature may vary significantly, the impact of these parameters on the sensor performance should be considered. In the future, a more in-depth analysis will be conducted to characterize the hysteresis effect in the humidity-relative capacitance change relationship and to study the sensor behavior over a wide range of temperatures.

f) Dynamic operating range of the sensor: In Section III-D, the influence of variations in sensor strain rate is explored. It was shown that an increase in the strain rate leads to an increase in stress in the loading part of the hysteresis curve. Furthermore, it was noted that the relative capacitance change increases with an increase in strain rate. Therefore, if the sensor is considered for applications where the dynamic behavior cannot be considered "quasi-static", it is advisable to determine the maximum strain rate to which the sensor will be subjected and analyze its potential impact on its performance. In applications where the force is to be measured through the capacitance values of the sensor, two components of the force applied to the sensor should be considered: a dynamic component and a "quasi-static" component.

g) Mechanical and electrical response design guideline: In section III-H, guidelines are established to assist designers in understanding the parameters that impact the sensor performance. These guidelines aim to facilitate the seamless integration of the sensor into the device envisioned by the designer. Nevertheless, using only these guidelines, it is difficult to predict the characteristics of the sensors with precision because of the non-linear response of the sensor. In the future, the development of a more precise model of the sensor is planned.

VI. Conclusions

In this research, we presented 3D-printed capacitive sensors using dielectric foam. The sensors can be manufactured using low-cost materials on multi-material extrusion 3D printers.

The sensors are parametric, and the analysis demonstrates that variations in density, infill, and dielectric foam anisotropy percentage change their sensitivity. Our approach allows for the creation of sensors with variable stiffnesses and thicknesses, catering to a wide range of application needs. Future work will focus on estimating sensor sensitivity considering the influence of foam parameters.

Furthermore, the integration of the proposed sensors into electronic devices within a single manufacturing process is demonstrated, including the use of conductive shields to mitigate the impact of capacitance disturbances. This lets us fabricate robust 3D-printed sensing devices with complex structures while maintaining control over their mechanical and electrical characteristics.

REFERENCES

[1] M. Bächer *et al.*, "Spin-it: Optimizing moment of inertia for spinnable objects," *Commun. ACM*, vol. 60, no. 8, p. 92–99, jul 2017.

[2] T. Kuipers *et al.*, "Crossfill: Foam structures with graded density for continuous material extrusion," *Computer-Aided Design*, vol. 114, pp. 37–50, 2019.

[3] T. Tricard *et al.*, "Freely orientable microstructures for designing deformable 3d prints," *ACM Trans. Graph.*, vol. 39, no. 6, nov 2020.

[4] X. Dong *et al.*, "4d printing of electroactive shape-changing composite structures and their programmable behaviors," *Composites Part A: Applied Science and Manufacturing*, vol. 157, p. 106925, 2022.

[5] Z. Qin *et al.*, "The mechanics and design of a lightweight three-dimensional graphene assembly," *Science Advances*, vol. 3, no. 1, p. e1601536, 2017.

[6] M. Schmitz *et al.*, "Capricate: A fabrication pipeline to design and 3d print capacitive touch sensors for interactive objects," in *Proc. of the ACM Symposium on User Interface Software & Technology*, 2015, p. 253–258.

[7] V. Savage *et al.*, "Sauron: embedded single-camera sensing of printed physical user interfaces," in *Proc. of the 26th Annual ACM Symposium on User Interface Software and Technology*, 2013, p. 447–456.

[8] M. Bächer *et al.*, "Defsense: Computational design of customized deformable input devices," in *Proc. of the 2016 CHI Conference on Human Factors in Computing Systems*, 2016, p. 3806–3816.

[9] A. Raj *et al.*, "Advancements in material extrusion based three-dimensional printing of sensors: a review," *International Journal on Interactive Design and Manufacturing (IJIDeM)*, vol. 18, no. 2, pp. 627–648, 2024.

[10] Z. Wang *et al.*, "A magnetic soft robot with multimodal sensing capability by multimaterial direct ink writing," *Additive Manufacturing*, vol. 61, p. 103320, 2023.

[11] T. Košir *et al.*, "Manufacturing of single-process 3d-printed piezoelectric sensors with electromagnetic protection using thermoplastic material extrusion," *Additive Manufacturing*, vol. 73, p. 103699, 2023.

[12] G. Wolterink *et al.*, "Evaluation of a 3d printed soft sensor for measuring fingertip interaction forces," *IEEE Sensors Journal*, vol. 22, no. 12, pp. 11 499–11 508, 2022.

[13] G. Stano *et al.*, "One-shot additive manufacturing of robotic finger with embedded sensing and actuation," *The International Journal of Advanced Manufacturing Technology*, vol. 124, pp. 467–485, 2023.

[14] M. Rafiee *et al.*, "Multi-material 3d and 4d printing: A survey," *Advanced Science*, vol. 7, 2020.

[15] H. Sun *et al.*, "Highly conductive and stretchable filament for flexible electronics," *Additive Manufacturing*, vol. 78, p. 103872, 2023.

[16] A. Z. Stefanov *et al.*, "Fully fff-printed capacitive displacement sensor based on graphene/pla composite and thermoplastic elastomer filaments," *IEEE Sensors Journal*, vol. 22, no. 11, pp. 10 437–10 445, 2022.

[17] J. Oprel *et al.*, "Novel 3d printed capacitive shear stress sensor," *Additive Manufacturing*, vol. 73, p. 103674, 2023.

[18] J. A. Hernandez *et al.*, "The development and characterization of carbon nanofiber/polylactic acid filament for additively manufactured piezoresistive sensors," *Additive Manufacturing*, vol. 58, p. 102948, 2022.

[19] M. Arh *et al.*, "Experimental identification of the dynamic piezoresistivity of fused-filament-fabricated structures," *Additive Manufacturing*, vol. 36, p. 101493, 2020.

[20] J. Akmal *et al.*, "Additive manufacturing of self-sensing parts through material extrusion," *Virtual and Physical Prototyping*, vol. 19, no. 1, p. e2321200, 2024.

[21] B. M. Lee *et al.*, "Flexible multifunctional sensors using 3-d-printed pedot:pss composites," *IEEE Sensors Journal*, vol. 24, no. 6, pp. 7584–7592, 2024.

[22] D. Kosmas *et al.*, "Sensing by instrumented 3d printed pessary," in *2024 IEEE International Conference on Flexible and Printable Sensors and Systems (FLEPS)*, 2024, pp. 1–4.

[23] Y. Sellami *et al.*, "Piezoelectret sensors from direct 3d-printing onto bulk films," in *2023 IEEE SENSORS*, 2023, pp. 1–4.

[24] H. Zhang *et al.*, "One-step fabrication of highly sensitive pressure sensor by all FDM printing," *Composites Science and Technology*, vol. 226, p. 109531, 2022.

[25] H. Nassar *et al.*, "Fully 3d printed piezoelectric pressure sensor for dynamic tactile sensing," *Additive Manufacturing*, vol. 71, p. 103601, 2023.

[26] B. Latsch *et al.*, "3d-printed piezoelectric pla-based insole for event detection in gait analysis," *IEEE Sensors Journal*, vol. 24, no. 16, pp. 26 472–26 486, 2024.

[27] A. J. Cheng *et al.*, "Recent advances of capacitive sensors: Materials, microstructure designs, applications, and opportunities," *Advanced Materials Technologies*, vol. 8, no. 11, p. 2201959, 2023.

[28] J. Burstyn *et al.*, "Printput: Resistive and capacitive input widgets for interactive 3d prints," in *Human-Computer Interaction – INTERACT 2015*. Berlin, Heidelberg: Springer-Verlag, 2022, p. 332–339.

[29] M. Schmitz *et al.*, "Trilaterate: A fabrication pipeline to design and 3d print hover-, touch-, and force-sensitive objects," in *Proc. of the 2019 Conference on Human Factors in Computing Systems*, 2019, p. 1–13.

[30] K. Baek *et al.*, "3d printing-assisted soft capacitive inclinometers for simultaneous monitoring of tilt angles and directions," *IEEE Access*, vol. 10, pp. 31 445–31 454, 2022.

[31] A. Leoni *et al.*, "Analysis and development technique of a fully 3-d-printed differential capacitive anemometric sensor," *IEEE Sensors Journal*, vol. 22, pp. 19 439–19 454, 2022.

[32] M. Schmitz *et al.*, "Flexibles: Deformation-aware 3d-printed tangibles for capacitive touchscreens," in *Proceedings of the 2017 CHI Conference on Human Factors in Computing Systems*, ser. CHI '17. New York, NY, USA: Association for Computing Machinery, 2017, p. 1001–1014.

[33] J. Gong *et al.*, "Metasense: Integrating sensing capabilities into mechanical metamaterial," in *The 34th Annual ACM Symposium on User Interface Software and Technology*, ser. UIST '21. New York, NY, USA: Association for Computing Machinery, 2021, p. 1063–1073.

[34] J. Yu *et al.*, "Fabricating customizable 3-d printed pressure sensors by tuning infill characteristics," *IEEE Sensors Journal*, vol. 24, no. 6, pp. 7604–7613, 2024.

[35] R. Sakura *et al.*, "Lattisense: A 3d-printable resistive deformation sensor with lattice structures," in *Proceedings of the 8th ACM Symposium on Computational Fabrication*, ser. SCF '23. New York, NY, USA: Association for Computing Machinery, 2023.

[36] M. E. Imanian *et al.*, "3d printed flexible wearable sensors based on triply periodic minimal surface structures for biomonitoring applications," *Smart Materials and Structures*, vol. 32, p. 015015, 2022.

[37] M. Kaur *et al.*, "Toward a smart compliant robotic gripper equipped with 3d-designed cellular fingers," *Advanced Intelligent Systems*, vol. 1, p. 1900019, 2019.

[38] "Icesl: A slicer and modeler, https://icesl.loria.fr," 2013.

[39] J. Martínez *et al.*, "Polyhedral voronoi diagrams for additive manufacturing," *ACM Trans. Graph.*, vol. 37, no. 4, jul 2018.

[40] D. W. Abueidda *et al.*, "Mechanical properties of 3d printed polymeric gyroid cellular structures: Experimental and finite element study," *Materials & Design*, vol. 165, p. 107597, 2019.

[41] D. Halliday *et al.*, *Physics, Volume 2*. John Wiley & Sons, 2010.

[42] F. bo Zhu *et al.*, "Mechanics of dielectric elastomers: materials, structures, and devices," *Journal of Zhejiang University-SCIENCE A*, vol. 17, pp. 1–21, 2016.

[43] P. Lochmatter *et al.*, "Characterization of dielectric elastomer actuators based on a visco-hyperelastic film model," *Smart Materials and Structures*, vol. 16, no. 2, p. 477, 2007.

[44] M. Wissler *et al.*, "Electromechanical coupling in dielectric elastomer actuators," *Sensors and Actuators A: Physical*, vol. 138, pp. 384–393, 2007.

[45] O. Atalay *et al.*, "A highly sensitive capacitive-based soft pressure sensor based on a conductive fabric and a microporous dielectric layer," *Advanced Materials Technologies*, vol. 3, p. 1700237, 2018.

[46] H. J. Qi *et al.*, "Stress–strain behavior of thermoplastic polyurethanes," *Mechanics of Materials*, vol. 37, pp. 817–839, 2005.

[47] S. I. Reyes *et al.*, "Experimental characterization and constitutive modeling of thermoplastic polyurethane under complex uniaxial loading," *Journal of the Mechanics and Physics of Solids*, vol. 186, p. 105582, 2024.

[48] S. Jasmee *et al.*, "Hydrophobicity performance of polyethylene terephthalate (pet) and thermoplastic polyurethane (tpu) with thermal effect," *Materials research express*, vol. 5, no. 9, p. 096304, 2018.

[49] J. Zhang *et al.*, "Modeling of humidity effect on electromechanical properties of viscoelastic dielectric elastomer," *International Journal of Mechanical Sciences*, vol. 193, p. 106177, 2021.

[50] T. Vu-Cong *et al.*, "New operating limits for applications with electroactive elastomer: effect of the drift of the dielectric permittivity and the electrical breakdown," in *Electroactive Polymer Actuators and Devices (EAPAD) 2013*, vol. 8687. SPIE, 2013, pp. 479–491.

[51] G. Laput *et al.*, "Em-sense: Touch recognition of uninstrumented, electrical and electromechanical objects," in *Proceedings of the 28th Annual ACM Symposium on User Interface Software & Technology*, ser. UIST '15. New York, NY, USA: Association for Computing Machinery, 2015, p. 157–166.